Improved Photovoltaic Response of Nanocrystalline CdS-Sensitized Solar Cells through Interface Control

ARTICLE *in* ACS APPLIED MATERIALS & INTERFACES · MAY 2010

Impact Factor: 6.72 · DOI: 10.1021/am900917n · Source: PubMed

4 AUTHORS, INCLUDING:

Jae-Yeol Hwang
Institute for Basic Science (IBS), Center for …
42 PUBLICATIONS **254** CITATIONS
SEE PROFILE

Yong Hui Lee
École Polytechnique Fédérale de Lausanne
31 PUBLICATIONS **1,596** CITATIONS
SEE PROFILE

Sang Il Seok
Korea Research Institute of Chemical Tech…
48 PUBLICATIONS **1,174** CITATIONS
SEE PROFILE

Improved Photovoltaic Response of Nanocrystalline CdS-Sensitized Solar Cells through Interface Control

Jae-Yeol Hwang, Sang-A Lee, Yong Hui Lee, and Sang-Il Seok*

KRICT-EPFL Global Research Laboratory, Advanced Materials Division, Korea Research Institute of Chemical Technology, 19 Sinseongno, Yuseong, Daejeon 305-600, Korea

ABSTRACT Nanocrystalline CdS-sensitized solar cells (CdS-SSCs) based on mesoporous TiO_2 were fabricated by the spray pyrolysis deposition method. The energy conversion efficiency of these cells was drastically increased (156%) by modifying the junction structure through post-treatment that included soaking in a dilute $TiCl_4$ aqueous solution and subsequent thermal annealing. We propose that the post-treatment is responsible for an increased number of interconnections between TiO_2 and CdS, as well as surface passivation of the CdS sensitizer. The increase in the cell efficiency is attributed to the improved charge carrier transport, suppression of photoelectron recombination with holes both in the same sensitizer particle and in nearby ones, and suppression of photoelectron capture by the electrolyte.

KEYWORDS: CdS-sensitized solar cells • junction structure • post-treatment

1. INTRODUCTION

Mesoscopic sensitized solar cells (MSSCs) are one of the most promising alternatives for solar energy conversion into electrical energy (1). High-efficiency MSSCs are based on an extremely large surface area of TiO_2 electrode as compared with that of the flat structure employed in conventional solar cells. A large surface area facilitates the creation of a large number of junctions and an increase in the amount of sensitizer material that can be loaded on the TiO_2 surface, thereby leading to favorable light harvesting and collection of photogenerated charge carriers. The key factors determining the efficiency of MSSCs are the light-harvesting ability of the sensitizer attached to the surface of the TiO_2 matrix and the transport dynamics of photogenerated carriers (2, 3).

Recently, semiconductor nanocrystalline particles such as CdS (4), CdSe (5), and PbS (4, 6) that absorb visible or near-infrared light have been used as alternate sensitizers in MSSCs. Advantages of inorganic semiconductor sensitizers over conventional dyes are their high extinction coefficient and large intrinsic dipole moment that leads to rapid charge separation (7). In particular, quantum dots (QDs), a special class of semiconductor nanoparticles exhibiting the quantum confinement effect, enable us to tailor the optical properties such as the band gap by controlling the particle size. In addition, it has been reported that the process of multiple exciton generation (MEG) can occur under specific excitation conditions in semiconductor nanoparticles (8, 9). However, the efficiency of QD-sensitized solar cells (QDSSC) is still very low, and the reasons for this are not yet clearly understood. One of the possible reasons is the difficulty of assembling a sufficiently large number of QDs on a mesoporous TiO_2 matrix in order to obtain a well-covered monolayer without cluster formation or aggregation (10). Another reasons are the higher recombination rate between semiconductor nanoparticles (or QDs) and electrolytes and the presence of surface states (electron and hole traps) in the sensitizing semiconductors, which results in lower short-circuit current and open-circuit photovoltage (7, 11). The retardation of charge recombination between sensitizers and electrolytes and blocking of the surface states was achieved through the surface passivation of sensitizers by using ZnS (5, 7), amorphous TiO_2 layer (12), etc.

Apart from the efficiency, the cost-effectiveness of mass fabrication is equally important for solar cells. An economical assembling process for solar cell manufacture is the spray pyrolysis deposition (SPD) of sensitizers on TiO_2 electrodes, which is suitable for wide-area coating. In this paper, we present the enhancement of the photovoltaic characteristics of CdS-sensitized solar cells (CdS-SSCs) through the modification of junction structure by employing post-treatment, which includes thermal annealing of CdS-coated TiO_2 layers after soaking them in a dilute $TiCl_4$ aqueous solution.

2. EXPERIMENTAL SECTION

Commercially available glass substrate coated with F-doped SnO_2 (FTO) (Hartford glass; about 15 ohm/sq) was used as transparent conducting oxide (TCO) to prepare the TiO_2 photoelectrode. It was cleaned by successive immersion in acetone, deionized (DI) water, and ethanol in an ultrasonic cleaner before cell fabrication.

In order to eliminate the parasitic effect due to the direct carrier recombination occurring at the FTO substrate-electrolyte interface, a thin TiO_2 blocking layer of about 10 nm was deposited on the FTO substrate by spray pyrolysis, as described elsewhere (13). A mesoporous nanocrystalline TiO_2 matrix was

* Corresponding author. E-mail: seoksi@krict.re.kr.
Received for review December 22, 2009 and accepted April 15, 2010
DOI: 10.1021/am900917n

prepared on the FTO substrate by screen printing of TiO_2 paste (Degussa P25), followed by annealing at 500 °C for 30 min in air (14). The thickness and crystallite size of the film, measured using a surface profiler and a scanning electron microscope, were 5 μm and 25−30 nm, respectively.

Chemical reagents were used as-procured, i.e., without further purification. A CdS precursor solution was prepared from reagent-grade $CdCl_2$ (Aldrich) and thiourea (Aldrich). A transparent clear aqueous solution containing $CdCl_2$ (0.1 M) and thiourea (1 g/100 mL) was sprayed on to the TiO_2/FTO film. To form interpenetrating networks between TiO_2 and CdS, the mixture solution was sprayed by glass nozzle (Wheaton TLC Reagent Sprayer) with a compressed N_2 onto the mesoporous TiO_2/FTO film heated on a hot plate of 400 °C. The distance between the spray nozzle and the substrate was 20 cm, and the N_2 pressure was 0.06 MPa. The spray was done for 2 s and stopped for 10 s, because the mist cooled the substrate. On increasing the spraying times of CdS, the color of the mesoporous TiO_2/FTO film changed from white to deep yellow.

The prepared mesoporous TiO_2/FTO photoelectrode was subjected to post-treatment before or after CdS was deposited on it by spray pyrolysis. The post-treatment included soaking in a 40-mM $TiCl_4$ aqueous solution at room temperature for 50 min followed by a thermal annealing at 500 °C for 30 min. A cell was fabricated by combining the CdS-sensitized TiO_2 electrode and a Pt-coated counter electrode using 60-μm-thick sealing material (Surlyn 1702, DuPont). A solution containing 0.60 M butylmethylimidazolium iodide (BMII), 0.03 M I_2, 0.1 M guanidinium thiocyanate, and 0.5 M 4-tert-bythylpyridine in the mixture of acetonitrile and valeronitrile with a volume ratio of 85:15 was used as the redox electrolyte. The electrolyte was introduced by vacuum backfilling, prior to finishing hole sealing. To improve electrical contact, lead contact pads were made on both sides of electrodes by using an ultrasonic soldering iron. The surface area of the photoelectrode was found to be 0.18 cm^2.

The crystallinity of CdS was investigated using an X-ray diffractometer (Rigaku rint-2000). The absorption spectrum and optical band gap of spray-pyrolyzed CdS films were investigated with a UV−vis spectrophotometer. The microstructures of the CdS-deposited TiO_2 electrode after soaking it in a dilute $TiCl_4$ solution and annealing at 500 °C were observed using a transmission electron microscope (TEM) (FEI, Tecnai G2) operating at 200 kV, together with energy-dispersive X-ray (EDX) analysis.

The photocurrent−voltage (I−V) curves were obtained under the illumination from a solar simulator (Newport, Class A, 91195A) at one sun (AM 1.5G, 100 mW/cm^2) by a Keithley 2420 source meter equipped with a calibrated Si-reference cell (certified by NREL). The external quantum efficiencies (EQE) of solar cells were analyzed using a fully computerized homemade measurement system consisting of a 300-W xenon lamp (Newport), a monochromator (Newport cornerstone 260), and a multimeter (Keithley 2002). The photon flux of light incident on the samples was calibrated using a silicon photodiode. Measurements were typically made at 5 nm wavelength intervals between 350 and 700 nm. To eliminate experimental errors, three different cells with the same structure were fabricated using the same procedure, and all measurements were carried out five times and averaged.

3. RESULTS AND DISCUSSION

Figure 1 shows the powder XRD patterns of a FTO substrate and the CdS layers deposited on it by the spray pyrolysis method using a mixture solution of $CdCl_2$ and thiourea and different spraying times. All the peaks are assigned to a hexagonal CdS phase without any secondary phase at a substrate temperature of 400 °C. The structural

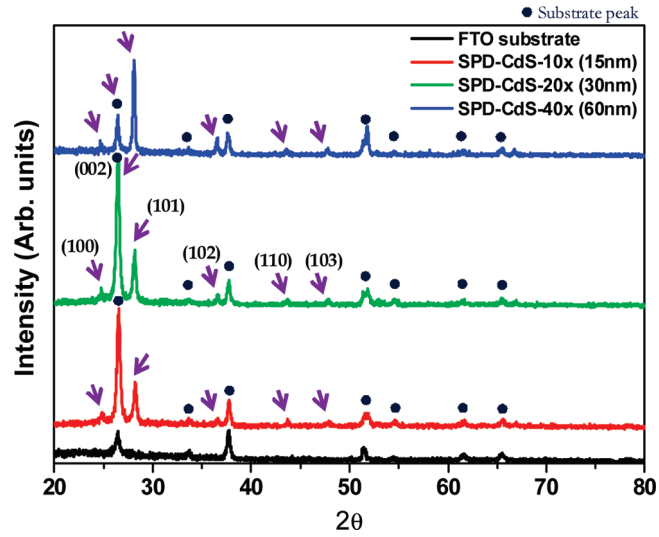

FIGURE 1. XRD patterns of CdS layers deposited on FTO substrates by the spray pyrolysis method, shown as a function of spray times at a substrate temperature of 400 °C.

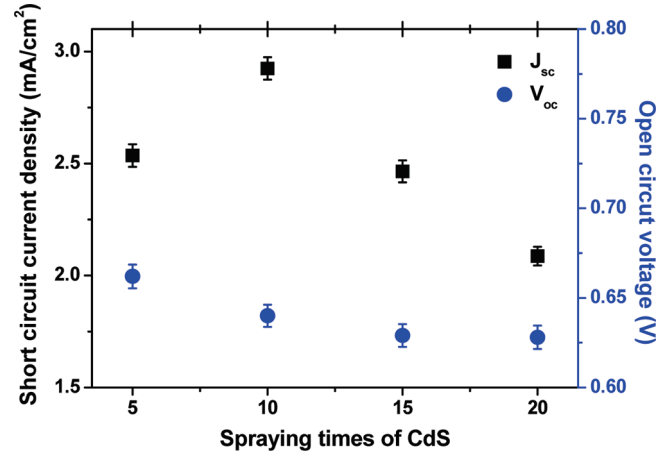

FIGURE 2. J_{sc} and V_{oc} of CdS-sensitized solar cells, measured as a function of spray times of CdS. The device structure is the same as that of Cell-(I).

and optical properties of the CdS layers deposited at the substrate temperatures of 400, 450, and 500 °C were found to be the same. From these results, the deposition temperature of CdS was set to be 400 °C for the sensitization of the mesoporous TiO_2 matrix. We surmise that spray-processed nanocrystalline CdS is thermally stable in this temperature range.

It is known that in a DSSC, with an increase in the thickness of the TiO_2 film, the photocurrent increaeses because of an increase in the amount of adsorbed dye. However, an increased film thickness induces diminution of the open-circuit voltage because of an increase in the dark current, which is proportional to the surface area of the film (15). A similar observation was made in the present CdS-SSC investigation. Further, a fully stained CdS/TiO_2 matrix was obtained by SPD on a 5 μm thick TiO_2 matrix. From this experimental observation, the thickness of the TiO_2 layer was set to be 5 μm.

Figure 2 shows the variations in the short-circuit photocurrent density (J_{sc}) and the open-circuit voltage (V_{oc}) of CdS-SSCs with CdS spraying times. From this figure, it is observed

that V_{oc} decreases linearly with the number of deposition cycles of CdS, whereas J_{sc} significantly increases (up to 10 deposition cycles) and then decreases. Here, J_{sc} can be described by eq 1, where q is the elementary charge, I_o is the incident photon flux of light (6.6×10^{16} cm^{-2}s^{-1}), η_{lh} is the light-harvesting efficiency of a cell, and η_{inj} is the charge-injection efficiency. η_{cc} is the charge collection efficiency, which is determined by the competition between recombination and charge collection. The product of three parameters ($\eta_{lh}\eta_{inj}\eta_{cc}$) is commonly referred to as the incident photon-to-current conversion efficiency (16)

$$J_{SC} = q\eta_{lh}\eta_{inj}\eta_{cc}I_o \quad (1)$$

On the basis of the results shown in Figure 2, the number of optimum spray times of CdS was set to be 10, corresponding to a CdS thickness of 15 nm. The thickness (or particle size) of CdS was estimated from that of a CdS layer deposited on an FTO substrate under the same conditions. We believe that the decrease in J_{sc} and V_{oc} values is due to an increase in the number of the aggregated CdS particles on the surface of the mesoporous TiO_2 matrix, resulting in the recombination of carriers. During the initial stages of the formation of a CdS coating on a TiO_2 matrix, the CdS nanoparticles form a monolayer on the TiO_2 surface. However, after the monolayer formation, any additional coatings of CdS particles will lead to particle aggregation, and the CdS particles without making any contact with the underlying mesoporous TiO_2 matrix, depending on the surface morphology and the states of the photoelectrode. In other words, these aggregated CdS particles have no direct connection with the TiO_2 matrix and may eventually become recombination centers for photoelectrons that recombine with the holes existing in either the same CdS particle or the electrolyte. Such sensitizers might not contribute to light harvesting and give photogenerated electrons to TiO_2, and become one of the potential recombination centers in a system. Further, it is well-known that Ru-complex dye acts like an electron-blocking layer and helps reduce the carrier recombination occurring between TiO_2 and the electrolyte in DSSCs, even in the event of dye aggregation (17). On the contrary, the recombination process at the CdS-electrolyte junction in CdS-SSCs might be a potentially serious pathway, because of significant differences between dyes in terms of surface bonding states, electronic configurations, conductivities, electron mobilities, and electron-blocking characteristics to prevent back electron transfer between CdS and electrolytes (11). In particular, in the presence of aggregated CdS particles on TiO_2, the recombination of charge carriers with those in either the same CdS particle or the electrolyte can be a dominant process, responsible for a low efficiency in cell performance, as compared to charge collection and/or propagation of photogenerated electrons. This implies that the recombination at the junction between aggregated CdS particles and electrolyte is active and the contribution of this phenomenon is not negligible in CdS-SSCs. To investigate the effects of surface modification on charge injection and recombination

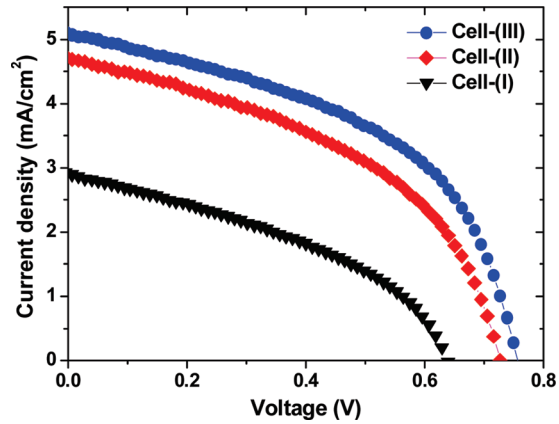

FIGURE 3. $I-V$ characteristics of the CdS-sensitized solar cells with different junction structures of UL-TiO_2/CdS/TiO_2-electrolyte [Cell-(I)], UL-TiO_2/CdS/UL-TiO_2/TiO_2-electrolyte [Cell-(II)], and CdS/UL-TiO_2/TiO_2-electrolyte [Cell-(III)] under simulated 1 sun irradiance (AM 1.5G, 100 mW/cm^2).

Table 1. Parameters Obtained from the $I-V$ Measurements (Figure 3) of the CdS-Sensitized Solar Cells

devices	J_{sc} (mA/cm^2)	V_{oc} (V)	FF (%)	efficiency (%)
Cell-I	2.92	0.64	39	0.73
Cell-II	4.72	0.73	45	1.55
Cell-III	5.17	0.77	47	1.87

in CdS-SSCs, we carefully designed and prepared three cells with different junction structures at CdS-TiO_2 and/or CdS/TiO_2-electrolyte interfaces. Before and after sensitization, TiO_2 photoelectrodes were subjected to pretreatment and post-treatment, respectively. Both these treatments were the same: The photoelectrodes were soaked in a dilute $TiCl_4$ aqueous solution and then annealed. The pretreatment and post-treatment were performed in order to change the junction structures by introducing ultrathin TiO_2 layers (UL-TiO_2) at CdS-TiO_2 and CdS/TiO_2-electrolyte interfaces, respectively. Three PV cells were designated as Cell-(I) ([the cell processed by pretreatment, i.e., before sensitization), Cell-(II) (the cell processed by both pre- and post-treatments, i.e., before and after sensitization), and Cell-(III) (the cell processed by post-treatment, i.e., after sensitization). As shown in Figure 3 and Table 1, after the junction structure at the CdS/TiO_2-electrolyte interface was modified by post-treatment, J_{sc}, V_{oc}, the fill factor, and cell efficiency of Cell-(II) were drastically increased by about 62, 14, 15, and 112%, respectively, as compared to those of Cell-(I). The maximal cell efficiency of the CdS-sensitized solar cell [Cell-(III)] is 1.87%, which is an improvement of 156% over that of Cell-(I), under simulated one-sun irradiation (AM 1.5G, 100 mW/cm^2). Furthermore, it was found that a photostability of CdS-SSSs was greatly improved by employing post-treatment. In the case of the Cell-(I) fabricated without post-treatment, the CdS nanoparticles as sensitizer were rapidly bleached after injecting the corrosive I^-/I_3^- electrolyte into the cell. The conversion efficiency of the cell is degraded in approximately half within 24 h. In contrast, both the Cell-(II) and Cell-(III) showed a stable performance even after several days of storage in ambient atmosphere. It was

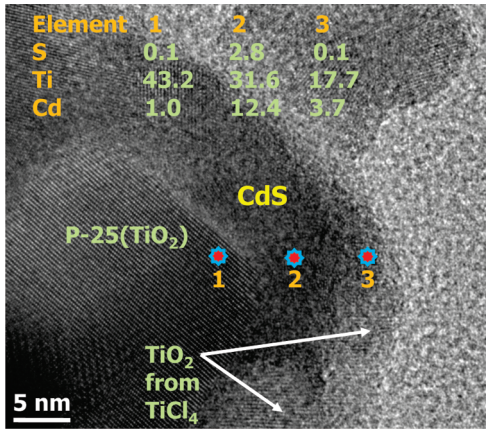

FIGURE 4. TEM image of a CdS-sensitized mesoporous TiO_2 electrode, recorded after post-treatment of the electrode by soaking it in a dilute $TiCl_4$ solution and annealing at 500 °C. Data obtained by energy-dispersive X-ray (EDX) analysis performed at three different positions is also shown.

previously reported (12) that the improved performance and photostabilty of the cells is related with the surface passivation of CdS by TiO_2 as a secondary phase.

Direct visualization of the CdS-sensitized electrode after modifying its junction structure at the CdS/TiO_2-electrolyte interface was performed by TEM, together with energy-dispersive X-ray (EDX) analysis data, recorded at three different distances. As can be seen in Figure 4, the results show the presence of a surface TiO_2 layer (or particles) on the CdS/TiO_2 photoelectrode; this layer is formed by the post-treatment. A similar observation in the improvement of cell performance of a CdS-sensitized solar cell was reported by M. Shalom et al. (12); they even applied amorphous TiO_2 layers on CdS sensitizes.

From the above discussions, we can assume that the η_{lh} values of Cell-(I) and Cell-(II) are same, and the main reason for the improvement in the photovoltaic responses is an increase in the product of η_{inj} and η_{cc} caused by the modification of the junction structure at the CdS/TiO_2-electrolyte interface. There are three possible explanations for the improvement achieved in the photovoltaic responses by modifying the junction structure at the CdS/TiO_2-electolyte interface through post-treatment. One reason is that charge injection is increased by the improved interconnecting networks between CdS and the mesoporous TiO_2 matrix, resulting in an increase in J_{sc}, η_{inj}, and η_{cc}. Another reason is a decrease in the number of defect states on the photoelectrode surface. The number of surface traps decreased because of the better coverage of CdS/TiO_2 surfaces with TiO_2, which diminished the back electron transfer from mesoporous TiO_2 to the electrolyte. Further, V_{oc} increased because of the inhibition of recombination and a possible decrease in the back electron transfer because back electron transfer is one of the major causes for V_{oc} decrease (18). Finally, the third reason is a decrease in carrier recombination between CdS/TiO_2 and the electrolyte. Charge transport in mesoporous a TiO_2-based solar cell system is well explained by the random-walk model (19). Photogenerated electrons can move freely on the surface of a mesoporous CdS/TiO_2 matrix. In the absence of a recombination barrier at the CdS/TiO_2-electrolyte junction, the recombination rate may be high, depending on the properties of the electrolyte, and the photogenerated electrons from CdS can easily recombine with the holes from the electrolyte. This can lead to a decrease in both J_{sc} and V_{oc}. If the surface of a CdS/TiO_2 photoelectrode is passivated by a TiO_2 layer (or particles) and/or the interconnections between CdS and TiO_2 are increased by post-treatment, the recombination probability and randomized movement of photogenerated electrons from CdS/TiO_2 to the electrolyte can be restricted and decreased. In CdS-SSCs, depending on the contribution of charge collection and the junction structure between CdS and the TiO_2 matrix, CdS sensitizers can be defined and categorized into two types: active sensitizers (CdS in directly contact with the TiO_2 matrix) and inactive sensitizers (vice versa). In the case of an inactive sensitizer, injecting photogenerated electrons from CdS to the mesoporous TiO_2 matrix might be very difficult because of the absence of direct interconnection between CdS and TiO_2. Therefore, an inactive sensitizer is one of the possible recombination centers for carriers in a CdS/TiO_2 system. It was reported that the $TiCl_4$ treatment covers a rather impure core with a thin layer of highly pure TiO_2 and leads to an epitaxial growth of TiO_2 particles having a radius of about 1 nm, which results in an improvement in the injection efficiency, and the blocking character of the semiconductor-electrolyte junction (14, 20). The newly generated TiO_2 particles (resulting from the hydrolysis of $TiCl_4$) make new interconnections with aggregated CdS and thereby convert the "inactive" sensitizer to an "active" sensitizer. This transformation of an inactive sensitizer into an active sensitizer results because of the formation of TiO_2 particles between aggregated CdS particles. These structural changes provide additional pathways to transfer the photogenerated electrons at CdS−TiO_2 and TiO_2−TiO_2 junctions, resulting in a decrease in the recombination rate at the CdS-electrolyte interface and an increase in J_{sc}, V_{oc}, and the charge injection efficiency (η_{inj}).

To reconfirm the effect of junction modification, carried out by post-treatment, on the photovoltaic characteristics, we compared the J_{sc} and V_{oc} values of Cell-(II) and Cell-(III). Both J_{sc} and V_{oc} values of Cell-(III) are higher than those of Cell-(II). We believe that this superior photovoltaic property of Cell-(III) is related to the quantitative difference between the active CdS sensitizer and the internal CdS-TiO_2 junctions. Because the surface area and pore size of the mesoporous TiO_2 matrix in Cell-(III) are larger than those of the TiO_2 matrix in Cell-(II), more interpenetrating and interconnecting networks between CdS and TiO_2 can be made in Cell-(III) by post-treatment than in Cell-(II). Y. Ogomi et al. reported a similar positive shift of an $I-V$ curve (increases in both V_{oc} and I_{sc}, as shown in Figure 3) caused by a better surface coverage of TiO_2 with dye molecules through dye uptake under pressurized CO_2 in a DSSC (21). Adsorption of the dye suppressed the dark current because the dye itself functioned as an effective recombination barrier on TiO_2. This explanation is consistent with our experimental findings and

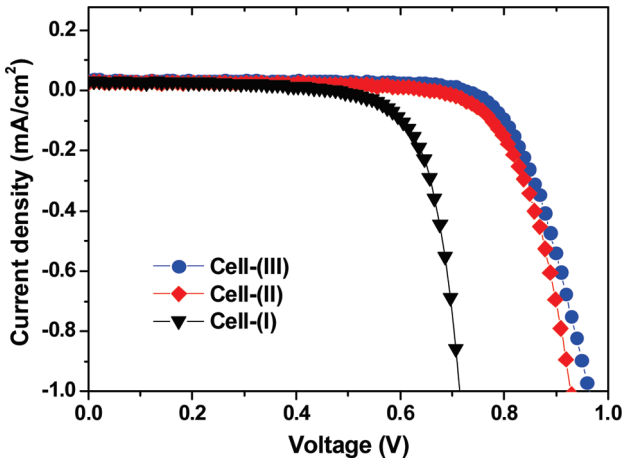

FIGURE 5. Photocurrent−voltage ($I-V$) characteristics under dark using UL-TiO_2/CdS/TiO_2-electrolyte [Cell-(I)], UL-TiO_2/CdS/UL-TiO_2/TiO_2-electrolyte [Cell-(II)], and CdS/UL-TiO_2/TiO_2-electrolyte [Cell-(III)].

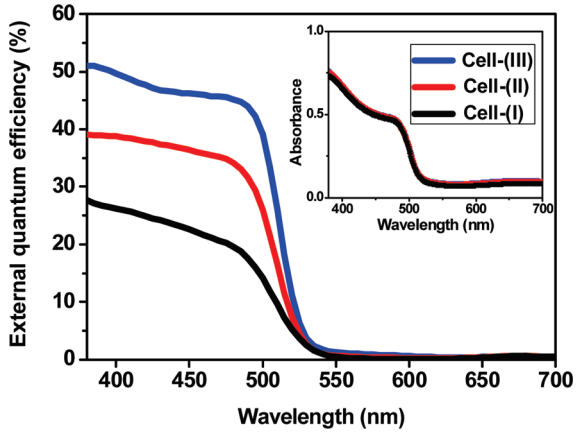

FIGURE 6. External quantum efficiencies of CdS-sensitized solar cells with different junction structures at their CdS/TiO_2-electrolyte interfaces. The inset shows the absorption spectrum of photoelectrodes for all cells.

the causes of improvements in photovoltaic characteristics through the modification of the junction structure in CdS-SSCs, regardless of the differences in the chemical and physical properties of the sensitizer and the recombination barrier.

The dark currents of all the cells were measured to further support the reasons for the improved photovoltaic characteristics. Figure 5 shows the dark current responses obtained for CdS-SSCs when the surface treatment was varied. The onset potential of the dark current for both the post-treated cells [Cell-(II) and Cell-(III)] was higher than that observed for Cell-I that was not post-treated. The dark current depends on the recombination rate between the electrons in the conduction band and the triiodide ions (I_3^-) in the electrolyte. Hence, retarding back electron transfer and preventing the recapture of photogenerated electrons by I_3^- are critical to obtain high V_{oc} (22, 23).

Figure 6 shows the external quantum efficiency (EQE) for three differently processed cells. The peak positions and the shapes of the EQE curves were identical for all the cells. However, the parallel positive shift of EQE curves was observed for Cell-(II) and Cell-(III). This can be interpreted as the evidence of the chemical and thermal stability of spray-deposited CdS and the absence of intermetallic compounds or a secondary phase after post-treatment. The photon-to-electron conversion behavior of CdS in EQE (about 525 nm) is almost the same as the absorption spectra (inset of Figure 6) of the photoelectrode. This implies that spray-deposited nanocrystalline CdS particles possess their intrinsic absorption band, and there are no size and quantum effects of the CdS sensitizer in this system. The EQE values of Cell-(II) and Cell-(III) were consistently higher in the entire spectral region as compared to that of Cell-(I), congruent with their higher $I-V$ parameters than those of Cell-(I). From these experimental observations, we surmise that the enhancement of photovoltaic performance of CdS-SSCs by surface modification is due to the increased charge injection and the decreased carrier recombination at photoelectrode−electrolyte junctions. The endeavors to make further enhancements in CdS-based solar cells by surface modification with post-treatments are underway. In addition, practical issues such as potential instability of CdS in the iodide electrolyte will be resolved by using new electrolytes.

4. CONCLUSION

CdS-sensitized solar cells were fabricated by the spray pyrolysis deposition method. The junction structure of a cell was modified by post-treatment, which included thermal annealing of the CdS-coated mesoporous TiO_2 layer after soaking it in a dilute $TiCl_4$ aqueous solution. The photovoltaic responses, such as J_{sc} and V_{oc}, were drastically increased by the modification of the junction structure. We surmise that these improvements are mainly due to an increase in the number of interconnections between CdS and the TiO_2 matrix and the retardation of the carrier recombination rate. The microstructural modification carried out at the CdS-TiO_2 and CdS/TiO_2-electrolyte junctions by the post-treatment was found to be an effective method to improve photovoltaic characteristics without changing the host structure. It was experimentally confirmed that the spray-pyrolyzed nanocrystalline CdS sensitizer was thermally stable up to 500 °C. This provides the cell fabrication under high temperature, which is suitable for successive deposition, sensitization, and treatment of each layer in tandem solar cells, inorganic/organic hybrid solar cells, multilayer structured solar cells, etc.

Acknowledgment. This study was supported by the Global Research Laboratory (GRL) Program through the National Research Foundation of Korea funded by the Ministry of Education, Science and Technology, Republic of Korea.

REFERENCES AND NOTES

(1) Grätzel, M. *Acc. Chem. Res.* **2009**, *42*, 1788.
(2) Cao, F.; Oskam, G.; Meyer, G. J.; Searson, P. C. *J. Phys. Chem.* **1996**, *100*, 17021.
(3) Nazeeruddin, M. K.; Pechy, P.; Renouard, T.; Zakeeruddin, S. M.; Humphry-Baker, R.; Comte, P.; Liska, P.; Cevey, L.; Costa, E.; Shklover, V.; Spiccia, L.; Deacon, G. B.; Bignozzi, C. A.; Grätzel, M. *J. Am. Chem. Soc.* **2001**, *123*, 1613.

(4) Lee, H. J.; Yum, J.-H.; Leventis, H. C.; Zakeeruddin, S. M.; Haque, S. M.; Chen, P.; Seok, S. I.; Grätzel, M.; Nazeeruddin, M. D. *Langmuir* **2009**, *25*, 7602.
(5) Lee, Y.-L.; Huang, B.-M.; Chin, H.-T. *Chem. Mater.* **2008**, *20*, 6903.
(6) Hyun, B.-R.; Zhong, Y.-W.; Bartnik, A. C.; Sun, L.; Abruna, H. D.; Wise, F. W.; Goodreau, J. D.; Matthews, J. R.; Leslie, T. M.; Borrelli, N. F *ACS Nano,* **2008**, *2*, 2206.
(7) Diguna, L. J.; Shen, Q.; Kobayashi, J.; Toyoda, T. *Appl. Phys. Lett.* **2007**, *91*, 023116.
(8) Beard, M. C.; Knutsen, K. P.; Yu, P.; Luther, J. M.; Song, Q.; Metzger, W. K.; Ellingson, R. J.; Nozik, A. J. *Nano Lett.* **2007**, *7*, 2506.
(9) Schaller, R.; Klimov, V. *Phys. Rev. Lett.* **2004**, *92*, 186601.
(10) Lee, H. Y.; Yum, J.-H.; Leventis, H. C.; Zakeeruddin, S. M.; Haque, S. A.; Chen, P.; Seok, S. I.; Gratzel, M.; Nazeeruddin, Md. K. *J. Phys. Chem. C* **2008**, *112*, 11600.
(11) Hodes, G. *J. Phys. Chem. C* **2008**, *112*, 17778.
(12) Shalom, M.; Dor, S.; Ruhle, S.; Grinis, L.; Zaban, A. *J. Phys. Chem. C* **2009**, *113*, 3895.
(13) Kavan, L.; Grätzel, M. *Electrochim. Acta* **1995**, *40*, 643.
(14) Nazeeruddin, M. K.; Kay, A.; Rodicio, I.; Humphry-Baker, R.; Muller, E.; Liska, P.; Vlachopoulos, N.; Grätzel, M. *J. Am. Chem. Soc.* **1993**, *115*, 6382.
(15) Boschloo, G.; Lindström, H.; Magnusson, E.; Holmberg, A.; Hagfeldt, A. *J. Photochem. Photobiol. A: Chem.* **2002**, *148*, 11.
(16) Franks, A. J.; Kopidakis, N.; Lagemaat, J. V. *Coord. Chem. Rev.* **2004**, *248*, 1165.
(17) Alex, S.; Santhosh, U.; Das, S. *J. Photochem. Photobiol. A: Chem.* **2005**, *172*, 63.
(18) Fabregat-Santiago, F.; García-Cañadas, J.; Palomares, E.; Clifford, J. N.; Haque, S. A.; Durrant, J. R.; Garcia-Belmonte, G.; Bisquert, J. *J. Appl. Phys.* **2004**, *96*, 6903.
(19) Nelson, J. *Phys. Rev. B* **1999**, *59*, 15374.
(20) Sommeling, P. M.; O'Regan, B. C.; Haswell, R. R.; Smit, H. J. P.; Bakker, N. J.; Smits, J. J. T.; Kroon, J. M.; van Roosmalen, J. A. M. *J. Phys. Chem. B* **2006**, *110*, 19191.
(21) Ogomi, Y.; Sakaguchi, S.; Kado, T.; Kono, M.; Yamaguchi, Y.; Hayase, S. *J. Electrochem. Soc.* **2006**, *153*, A2294.
(22) Ito, S.; Liska, P.; Comte, P.; Charvet, R.; Pechy, P.; Bach, U.; Schmidt-Mende, M.; Zakeeruddin, S. M.; Kay, A.; Nazeeruddin, M. K.; Grätzel, M. *Chem. Commun.* **2005**, 4351.
(23) Hara, K.; Dan-oh, Y.; Kasada, C.; Ohga, Y.; Shinpo, A.; Suga, S.; Sayama, K.; Arakawa, H. *Langmuir* **2004**, *20*, 4205.

AM900917N